

Multicolor Terahertz Frequency Mixer Using Multibunching of Free-Electron Beams

Weihao Liu,* Linbo Liang, Qika Jia, Lin Wang, and Yalin Lu

National Synchrotron Radiation Laboratory, University of Science and Technology of China, Hefei, Anhui 230029, China



(Received 2 November 2017; revised manuscript received 30 May 2018; published 17 September 2018)

We propose a free-electron-beam (FEB)-driven frequency mixer for generating terahertz-wave radiation. It employs an initial steady-current FEB to drive two cascaded gratings. On the first grating, the FEB is macrobunched by interacting with the self-stimulated backward slow waves. On the second grating, which operates at high harmonics of the first grating, it is further microbunched at high frequencies, producing mixed bunching components within the FEB. The multibunched FEB then generates a series of superradiant Smith-Purcell radiations from the second grating, achieving multicolor radiations in the terahertz region. The radiation can be tuned by adjusting the beam energy, covering the frequency range from 0.8 to 1.8 THz. It is a promising broad-tunable and multicolor terahertz source.

DOI: 10.1103/PhysRevApplied.10.034031

I. INTRODUCTION

Electromagnetic waves in the terahertz spectral range (from 0.1 to 10 THz) are very attractive to worldwide researchers since they have tremendous applications in modern science and technologies [1,2]. Yet, because of the lack of compact, high-power, and broad-tunable terahertz sources, many applications have been greatly limited [3,4]. The development of desirable terahertz sources has still been a challenge.

The solid-state electronic devices (SEDs) are efficient sources in the radio-frequency region, yet they are not capable of generating terahertz radiation directly because of material limitations. In practice, the frequency multipliers or mixers have to be applied to get radiation with frequency reaching the terahertz region. Yet, the output power is undesirable due to the low efficiency of traditional multipliers and mixers [5,6].

Compared with SEDs, the free-electron-beam (FEB)-driven radiation sources, the so-called vacuum electronic devices (VEDs), can achieve higher output power at microwave and millimeter-wave regions. Unfortunately, the VEDs also meet great challenges in the terahertz region: the radiation power and efficiency decrease dramatically as the frequency increases. One of the primary obstacles is the requirement of high beam current density [7,8], which is beyond the emission capability of available cathodes [9]. Applying a frequency multiplier to the VEDs seems to be a feasible solution since it could reduce the required beam current. Several attempts have been tried by

using closed slow-wave structures (SWSs) [10,11]. However, the applications of closed SWSs have been greatly limited by the low power capacity and manufacturing difficulties.

Recently, the radiation sources based on the well-known Smith-Purcell radiation (SPR) from open periodic structures [12–14], which avoid the disadvantages of closed SWSs, have gained increasing attention for generating terahertz radiation [15]. For example, the Orotron [16,17] (stimulated SPR within an open cavity) and the Smith-Purcell free-electron laser (SPFEL) [18–21] (coherent SPR from the harmonics of a self-bunched FEB) have achieved higher radiation frequency than the traditional VEDs. Yet, it is still difficult for them to reach high-frequency terahertz regions (such as higher than 0.5 THz). Using two cascade gratings has been proved to be an effective way to improve the performances of SPFEL. It can either enhance the radiation intensity by emitting the fundamental bunching component [22] or increase the frequency [23] by using higher harmonics.

In the present paper, we propose a type of frequency mixer, using the multibunching of a FEB on two cascade gratings to generate terahertz radiation. Its operation mechanism is essentially different from that of previous SPFELs with two cascade gratings and can be described as follows. The initial direct-current (dc) FEB is macrobunched by the first grating and further microbunched by the second one, producing frequency-mixed bunching components, which then generate coherent SPR from the second grating. The intense starting current density required in traditional VEDs and SPFELs is greatly reduced by setting the second grating to operate at the harmonics of the first one. Compared with the frequency-mixing methods used in tra-

*liuhao@ustc.edu.cn

ditional SEDs and VEDs, it could simultaneously generate coherent radiation with a series of frequencies (multicolor). Also, its radiation frequency can be tuned from 0.8 to 1.8 THz by adjusting the electron energy of the FEB. Thus, it affords an efficient way for developing compact, multicolor, and broad-tunable terahertz sources.

II. MODEL DESCRIPTION

A diagram of the proposed scheme is illustrated in Fig. 1. A continuous dc FEB successively passes over two rectangular conductor gratings with different sizes. The first grating with a big size is to prebunch the FEB, which is self-bunched (macrobunched) by interacting with backward surface waves (BSW) on the grating [24], just like the backward wave oscillator (BWO). The dominant (fundamental) bunching frequency (ω_1) is exactly the operation frequency of the BSW. Along with the self-bunching process, a train of electron bunches are produced within the FEB [10]. Besides the fundamental bunching components, high harmonics are also generated. Thus, the bunching factor of the self-bunched FEB could be expressed as

$$F_0 = F_1 e^{j\omega_1 t} + F_2 e^{j2\omega_1 t} + F_3 e^{j3\omega_1 t} + \dots, \quad (1)$$

in which F_m ($m = 1, 2, 3, \dots$) signifies the bunching factor of the m th harmonic component.

When passing over the second grating, which operates at one of the high harmonics of the fundamental bunching frequency ($\omega_2 = m\omega_1$), the FEB further interacts with the BSW on the second grating at a higher frequency (ω_2) and be further bunched (microbunched). As the beam-wave interaction reaches saturation, the microbunched component (ω_2), together with its harmonics, becomes significant. These microbunched components then mix with the macrobunched ones, generating a series of mixed bunched components in the FEB. The bunching factor under this condition can be expressed as

$$F = \sum F_s e^{j\omega_s t} = \sum \sum F_{p,q} e^{j(p\omega_1+q\omega_2)t}, \quad (2)$$

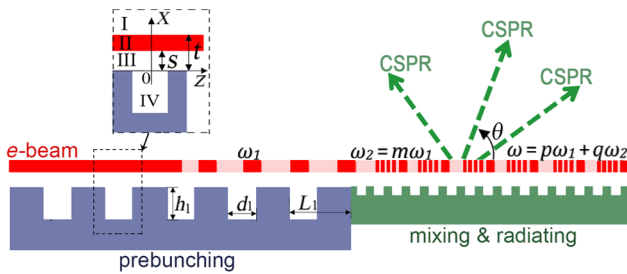


FIG. 1. Diagram of the proposed scheme. Here, CSPR denotes coherent Smith-Purcell radiation and θ signifies the radiation angle relative to the beam velocity. The inset shows the coordinates and the field regions used in theoretical analyses.

where $\omega_s = p\omega_1 + q\omega_2$ (p and q are integers) denotes the frequency of the mixed bunching component. Note that, here, the mixing is obtained by linear combinations of the fundamental component and its high harmonics.

The multibunched FEB generates coherent radiation in the upper space of the second grating via the superradiant Smith-Purcell effect [25]. The radiating wavelength and direction satisfy the SPR relation:

$$\lambda = L(1/\beta - \cos \theta)/|n|, \quad (3)$$

in which λ denotes the wavelength in the space, L is the structure period of the grating, n is a negative integer, $\beta = v_e/c$, v_e is electron velocity, c is the speed of light in the vacuum, and θ signifies the radiation angle relative to electron velocity as shown in Fig. 1. We note that only the mixed bunching components with frequencies being higher than the fundamental frequency of the second grating (ω_2) can satisfy Eq. (3) and generate superradiant SPR from the second grating, which actually works as a modified SPFEL driven by prebunched FEB. Compared with that of the dc beam, the required start current density of the prebunched beam is much lower, since the beam-wave interaction starts from the coherent radiation from a train of macrobunches, rather than from the incoherent radiation of a dc beam.

It should be noted that the mechanism of the proposed scheme is essentially different from that of previous SPFELs with two cascade gratings presented in Refs. [22] and [23]. In Ref. [22], the first double grating was to prebunch the initial dc beam, which is similar to the first grating used in our present scheme. Yet, on the second grating of that model, the prebunched beam was not further microbunched and there was no remarkable mixed bunching component in the radiation. Instead, the prebunched beam generated spontaneous coherent SPR from the second grating. The purpose of the second grating is either to change the radiating order [n in Eq. (3)] from $|n| > 1$ to $|n| = 1$ or to radiate the fundamental prebunching component, by which the radiation intensity could be enhanced. As for the scheme of [23], the second grating operates in the radiative region; namely, there is no surface wave excited by the FEB on the second grating, such that the prebunched beam cannot be further microbunched by the beam-wave interaction. The main function of the second grating with small size in Ref. [23] is to radiate one of the higher harmonics of the prebunching frequency via spontaneous coherent SPR and there are no mixed components for radiating, similarly to that in Ref. [22].

III. FORMULA DERIVATION

In this section, we derive the equations describing the beam-wave interactions and the dispersion relation governing the electromagnetic waves propagating along

the gratings. For the two-dimensional model considered in the present paper, the whole space could be divided into four regions according to boundaries; see the inset of Fig. 1. We write down the field expressions in each region and then apply them to the mode-matching method.

In order to satisfy the periodic boundary conditions, the fields above the grating should be expanded into infinite space-harmonics according to the Floquet's theorem. Thus, the fields in region I (the upper vacuum region; see Fig. 1) should be expressed as

$$\begin{cases} E_z^I = \sum_{n=-\infty}^{\infty} A_n e^{-k_{xn}^I x} e^{-j k_{zn} z}, \\ E_x^I = \sum_{n=-\infty}^{\infty} A_n \frac{-j k_{zn}}{k_{xn}^I} e^{-k_{xn}^I x} e^{-j k_{zn} z}, \\ H_y^I = \sum_{n=-\infty}^{\infty} A_n \frac{-j \omega \varepsilon}{k_{xn}^I} e^{-k_{xn}^I x} e^{-j k_{zn} z}, \end{cases} \quad (4)$$

where $k_{xn}^{I2} = k_{zn}^2 - k_0^2$, $k_{zn} = k_z + 2n\pi/L$, $k_0 = \omega/c$ is the wave number in the vacuum, ω is the angular frequency, and ε is the permittivity of vacuum. A_n , B_n , C_n , D_n , F_n , and G in Eqs. (4)–(8) are the coefficients to be determined by boundary conditions. Note that, here, we only consider the transverse-magnetic (TM) waves in the z direction since they are the operation modes interacting with the FEB.

According to previous studies [24], the continuous FEB could be treated as a linear, isotropic, and moving plasma dielectric with relative dielectric function expressed by

$$\varepsilon_b = 1 + \chi = 1 - \frac{\omega_p^2}{\gamma^3 (\omega - \beta c k_{zn})^2}, \quad (5)$$

where χ is the effective polarization function, $\gamma = 1/\sqrt{1-\beta^2}$ is the Lorentz factor of the electron beam, $\omega_p^2 = n_e q^2 / \varepsilon m_e$ is the effective plasma frequency, q is the electron charge, m_e is the electron mass, $n_e = J_e/qv_e$ is electron density, and J_e is the current density of the FEB. Thus, the fields in the FEB (region II) can be expressed as

$$\begin{cases} E_z^{II} = \sum_{n=-\infty}^{\infty} (B_n e^{-k_{xn}^{II} x} + C_n e^{k_{xn}^{II} x}) e^{-j k_{zn} z}, \\ E_x^{II} = \sum_{n=-\infty}^{\infty} \left(B_n \frac{-j k_{zn}}{k_{xn}^{II}} e^{-k_{xn}^{II} x} + C_n \frac{j k_{zn}}{k_{xn}^{II}} e^{k_{xn}^{II} x} \right) e^{-j k_{zn} z}, \\ H_y^{II} = \sum_{n=-\infty}^{\infty} \left(B_n \frac{-j \omega \varepsilon \varepsilon_b}{k_{xn}^{II}} e^{-k_{xn}^{II} x} + C_n \frac{j \omega \varepsilon}{k_{xn}^{II}} e^{k_{xn}^{II} x} \right) e^{-j k_{zn} z}, \end{cases} \quad (6)$$

where $k_{xn}^{II2} = k_{zn}^2 - \varepsilon_b k_0^2$.

Similarly, the fields in the gap between the beam and grating (region III) can be expressed as

$$\begin{cases} E_z^{III} = \sum_{n=-\infty}^{\infty} \left(D_n e^{-k_{xn}^{III} x} + F_n e^{k_{xn}^{III} x} \right) e^{-j k_{zn} z}, \\ E_x^{III} = \sum_{n=-\infty}^{\infty} \left(D_n \frac{-j k_{zn}}{k_{xn}^{III}} e^{-k_{xn}^{III} x} + F_n \frac{j k_{zn}}{k_{xn}^{III}} e^{k_{xn}^{III} x} \right) e^{-j k_{zn} z}, \\ H_y^{III} = \sum_{n=-\infty}^{\infty} \left(D_n \frac{-j \omega \varepsilon}{k_{xn}^{III}} e^{-k_{xn}^{III} x} + F_n \frac{j \omega \varepsilon}{k_{xn}^{III}} e^{k_{xn}^{III} x} \right) e^{-j k_{zn} z}, \end{cases} \quad (7)$$

where $k_{xn}^{III2} = k_{zn}^2 - k_0^2 = k_{xn}^I 2$. For simplicity, we write both k_{xn}^{III} and k_{xn}^I as k_{xn} hereafter.

Considering that the groove width of the grating is much less than the operation wavelength ($d \ll \lambda$), the fields in the rectangular grooves (region IV) can be treated as transverse-electromagnetic (TEM) waves in the x direction [26], which is the lowest mode within the grooves:

$$\begin{cases} E_z^{IV} = G \frac{\sin[k_0(h+x)]}{\sin(k_0 h)}, \\ H_y^{IV} = G \frac{-j \omega \varepsilon \cos[k_0(h+x)]}{k_0} \frac{1}{\sin(k_0 h)}. \end{cases} \quad (8)$$

The tangential fields should satisfy the following continuity conditions at interfaces of adjacent regions:

$$\begin{cases} E_z^I \Big|_{x=t} = E_z^{II} \Big|_{x=t}, \\ H_y^I \Big|_{x=t} = H_y^{II} \Big|_{x=t}, \end{cases} \quad (9)$$

$$\begin{cases} E_z^{II} \Big|_{x=s} = E_z^{III} \Big|_{x=s}, \\ H_y^{II} \Big|_{x=s} = H_y^{III} \Big|_{x=s}, \end{cases} \quad (10)$$

$$\begin{cases} E_z^{III} \Big|_{x=0} = \begin{cases} E_z^{IV} \Big|_{x=0}, & -d/2 < z < d/2, \\ 0, & d/2 < z < L - d/2, \end{cases} \\ \int_{-d/2}^{d/2} H_y^{III} \Big|_{x=0} dz = \int_{-d/2}^{d/2} H_y^{IV} \Big|_{x=0} dz. \end{cases} \quad (11)$$

In Eq. (11), the average matching condition for the tangential magnetic field is used [26]. Substituting Eqs. (4)–(8) into Eqs. (9)–(11) and after complicated but straightforward arithmetical operation, we can obtain the following dispersion equation:

$$\frac{d}{L} \sum_{n=-\infty}^{\infty} \frac{1 - Q_n}{1 + Q_n} \frac{1}{k_{xn}} \left[\frac{\sin(k_{zn} d/2)}{k_{zn} d/2} \right]^2 = \frac{1}{k_0 \tan(k_0 h)}, \quad (12)$$

in which

$$Q_n = - \frac{(\varepsilon_b k_{xn} + k_{xn}^I) e^{-k_{xn}s} \left[1 + \frac{\varepsilon_b k_{xn} - k_{xn}^I}{k_{xn}^I + \varepsilon_b k_{xn}} e^{2k_{xn}^I(s-t)} - \frac{2\varepsilon_b k_{xn}}{\varepsilon_b k_{xn} + k_{xn}^I} \right]}{(\varepsilon_b k_{xn} - k_{xn}^I) e^{k_{xn}s} \left[1 + \frac{\varepsilon_b k_{xn} - k_{xn}^I}{k_{xn}^I + \varepsilon_b k_{xn}} e^{2k_{xn}^I(s-t)} - \frac{2\varepsilon_b k_{xn}}{\varepsilon_b k_{xn} - k_{xn}^I} \right]}. \quad (13)$$

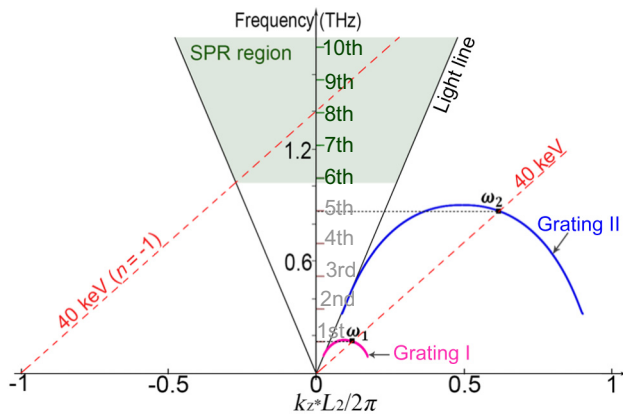


FIG. 2. Dispersion curves of both gratings and electron-beam lines. The shaded region indicates the SPR region for the 40-keV FEB on the second grating.

When the FEB is absent, the dispersion equation of grating can be obtained by letting $Q_n = 0$. The calculated dispersion curves of the lowest (primary) TM modes of two gratings are shown in Fig. 2, in which the structure parameters of two gratings are $L_1 = 0.4$ mm, $d_1 = 0.2$ mm, $h_1 = 0.3$ mm and $L_2 = 0.08$ mm, $d_2 = 0.04$ mm, $h_2 = 0.06$ mm, respectively. Namely, all parameters of the second grating are reduced by a factor of 5 compared to the first grating. It shows that when the electron energy of the FEB is 40 keV, the operating points (intersections of electron-beam lines with dispersion curves) of both gratings are located in the BSW regions, where the group velocities of surface waves are negative. Thus, the beam-wave interaction (bunching) can be self-stimulated (without external feedback) when the beam current of the FEB exceeds the start current on both gratings [13]. The operation frequency of the first grating (the macrobunching frequency) is 0.173 THz and that of the second grating (the microbunching frequency) is 0.865 THz, being the fifth harmonics of the macrobunching frequency ($\omega_2 = 5\omega_1$). Thus, the start current on the second grating is reduced according to previous analyses.

When interacting with the FEB, the self-excited BSW (operation modes) on the grating are amplified exponentially, which then leads to the bunching of the FEB in return. The growth rate is a key factor representing the beam-wave interaction and can be derived as follows. The dispersion equation of Eq. (12) has two variables: ω and k_z , the solutions of which are complex numbers. The imaginary part of one of the solutions indicates the growth rate [24]. To derive it, we rewrite Eq. (12) to be

$$f(\omega, k_z) = 0 \quad (14)$$

and then expand it about the synchronization (operation) point (ω_0, k_{z0}) on the dispersion curve:

$$f(\omega, k_z) = f(\omega_0, k_{z0}) + f_\omega \delta\omega + f_{k_z} \delta k_z + f_\chi \chi = 0, \quad (15)$$

in which $f_\omega = \partial f / \partial \omega$, $f_{k_z} = \partial f / \partial k_z$, and $f_\chi = \partial f / \partial \chi$ are the partial derivatives at the synchronization point; $\delta\omega = \omega - \omega_0$; and $\delta k_z = k_z - k_{z0}$. Considering $f(\omega_0, k_{z0}) = 0$ at the synchronization point and the following relation along the dispersion curve,

$$\frac{df}{dk_z} = 0 = f_{k_z} + \frac{\partial \omega}{\partial k_z} f_\omega = f_{k_z} + v_g f_\omega, \quad (16)$$

in which v_g is the group velocity, Eq. (15) can be simplified:

$$f(\omega, k_z) = f_\omega (\delta\omega - v_g \delta k_z) + f_\chi \chi = 0. \quad (17)$$

Substituting the polarization function χ in Eq. (5) into Eq. (17), we can get the following cubic equation:

$$(\delta\omega - v_g \delta k_z)^2 (\delta\omega - v_g \delta k_z) = \Delta = -\frac{\omega_p^2 f_\chi}{\gamma^3 f_\omega}. \quad (18)$$

The growth rate can then be obtained:

$$\tau = \text{Im}(\delta k_z) = \frac{\sqrt{3}}{2} \left| \frac{\Delta}{v_g^2 v_e} \right|^{1/3}. \quad (19)$$

The growth rate expressed by Eq. (19) holds true for both dc beams and prebunched beams, the difference of which lies in the initial condition. For the dc beam, the self-amplification starts from noise (incoherent spontaneous radiation), while for the prebunched beam, it starts from a seed (one of harmonics of the prebunching) with enhanced intensity [25], which exactly accounts for the reduce of start current.

IV. SIMULATION RESULTS

The start-to-end two-dimensional (2D) simulations of the proposed scheme are performed by applying the finite-difference-time-domain-(FDTD)-based fully electromagnetic code CHIPIC-2D [27]. In simulations, the conductivity of gratings is set to 2×10^7 S/m. The number of periods of the first grating is 40 and the second grating has 90 periods. The FEB is a sheet beam with a rectangular cross section, in which the y -directional width is much larger than the x -directional width. In 2D simulations, the y -directional widths of the FEB and of the grating are assumed to be infinite. The beam thickness in the x direction is 0.1 mm and the beam-to-grating distance is 0.01 mm. The initial beam current density is 50 A/cm², which is assumed to be uniformly distributed in the cross section of the FEB. An external uniform longitudinal magnetic field $B_z = 0.5$ T is used to transversely confine the FEB. We note that such sheet electron beams have been approximately achieved in experiments by several research groups [28–30].

Figure 3(a) illustrates the simulation-obtained phase-space distribution of the FEB when the beam-wave interaction is started. We note that the beam energy (velocity) is modulated by the first grating at a low frequency and then is further modulated by the second grating at a high frequency. Figure 3(b) further shows the particle distributions of the FEB, which is first macrobunched on the

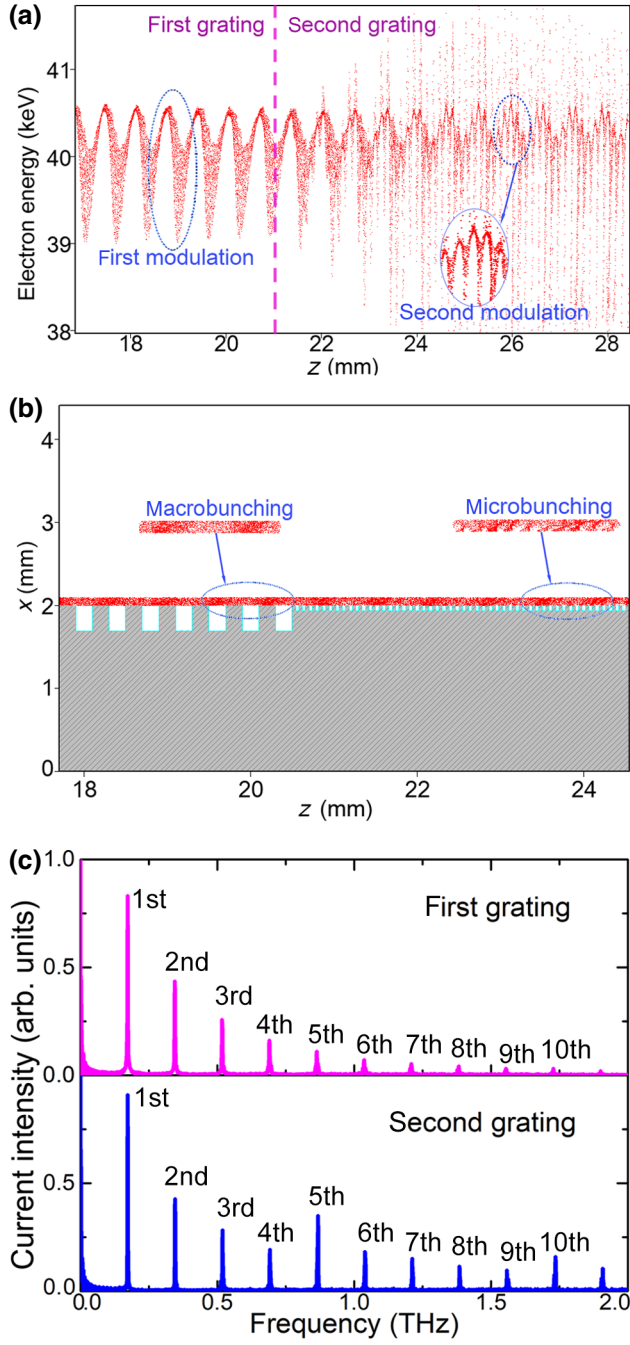


FIG. 3. (a) Simulation obtained phase-space distribution of the FEB with modulations. (b) Snapshot of the particle distribution of the FEB on both gratings. (c) Frequency spectra of the beam current density.

first grating and then microbunched on the second grating, agreeing well with theoretical predictions. We note that five microbunches are generated within each macrobunch. Figure 3(c) illustrates the frequency spectra of the beam current density (equivalent bunching factor) of the FEB. On the first grating, the bunching factor reaches peaks at the harmonics of the macrobunching frequency and the magnitude decreases quickly with the harmonic order. The intensities of harmonics higher than fifth order are so weak (the bunching factor is less than 0.1) that they cannot generate the desirable radiation power. After interacting with the second grating, the fifth harmonic (with microbunching frequency ω_2) is obviously enhanced; see the bottom subplot of Fig. 3(c). Also, other high harmonics (from sixth to tenth) are greatly (about five times) amplified because of the multibunching effect. Note that the tenth harmonic is enhanced more significantly than the eighth and ninth harmonics, which is because that it is the second harmonic of the microbunching frequency on the second grating. As illustrated in Fig. 2, the fifth harmonic is the surface wave propagating along the second grating, while the sixth to tenth harmonics are radiation waves since they are in the SPR region, and they are coherent radiations (superradiances) from the train of electron bunches [24,25].

To observe the radiation fields generated by the multibunched FEB, two detectors are placed at 4 mm above the second grating; see probe A (top left) and probe B (top right) in Fig. 4(a). Figure 4 presents the radiation spectra detected by two probes. It shows that the multicolor coherent radiation with a series of frequencies—from 0.865

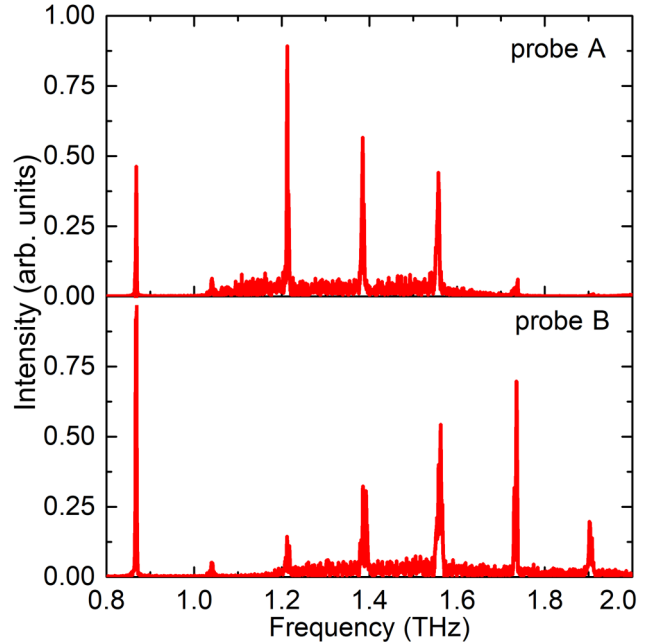


FIG. 4. Radiation spectra detected by probe A and probe B in the upper space of the second grating.

THz (fifth harmonic) to 1.73 THz (tenth harmonic)—is obtained. Note that, here, the probes can simultaneously detect the radiation at different directions since they are not infinitely far from the grating. It is different from the ideal case, where the observer is infinitely far from the grating and could only see the radiation from a single direction (radiation angle). For probe A, the radiations of the seventh to ninth harmonics are dominant, while for probe B, that of the eighth to tenth harmonics become dominant. This is because the radiation directions of different frequencies (harmonics) differ from each other according to the SPR relation: the radiation with a higher frequency has a smaller radiation angle (θ) when the radiation order (n) is the same according to Eq. (3). We note that the sixth harmonic is relatively weak, which is because its radiation is almost parallel to the grating and has not been effectively detected. The fifth harmonic component is radiated by the surface wave through both ends of the grating. Figure 5 further illustrates the field patterns (E_z component) above the second grating for different radiation harmonics in the frequency domain. The radiation angles of the sixth to ninth harmonics are, respectively, $\theta = 158.5^\circ$, $\theta = 115^\circ$, $\theta = 92^\circ$, and $\theta = 74^\circ$, all of which agree with the SPR relation of Eq. (3).

Now we consider the frequency tunability of the proposed scheme. According to the dispersion curves shown in Fig. 2, the operation frequencies of the first (macrobunching) and second (microbunching) gratings can both be changed by adjusting the beam energy. Their harmonic relationship ($\omega_2 = m\omega_1$) is kept in a certain region, which sets the base for the tunability of the radiation. For the present mode, the macrobunching frequency ranges from 0.15 to 0.18 THz as the electron energy of the FEB changes from 20 to 50 keV and the microbunching frequency is from 0.75 to 0.89 THz, being the fifth harmonics of the macrobunching ($\omega_2 = 5\omega_1$). The frequencies of mixed components are then changed accordingly. Figure 6(a) shows the simulation-observed radiation frequency of different harmonics as a function of beam energy. We note that the radiation frequency covers the region from 0.8 to 1.8 THz as the beam energy varies from 20 to 50 keV, indicating that it is a broad tunable terahertz source. Figure 6(b) presents the evaluated radiation power (by integrating the whole grating) versus frequency as the beam energy is being tuned (here, the grating width in the y direction is assumed to be 1 mm). It shows that the radiation power ranges from 10 to 60 mW within the frequency region of 0.8–1.8 THz. The relative maximum power is obtained at about 1 THz, which is from the sixth harmonic when the beam energy is about 50 keV. It can be explained that the beam-wave interaction reaches the highest efficiency when the operation point is close to the bragg point ($k_z L_{1,2} / 2\pi = 0.5$ in Fig. 2). It is worth noting that these are average powers since the dc beams are used and this average power level is higher than that of

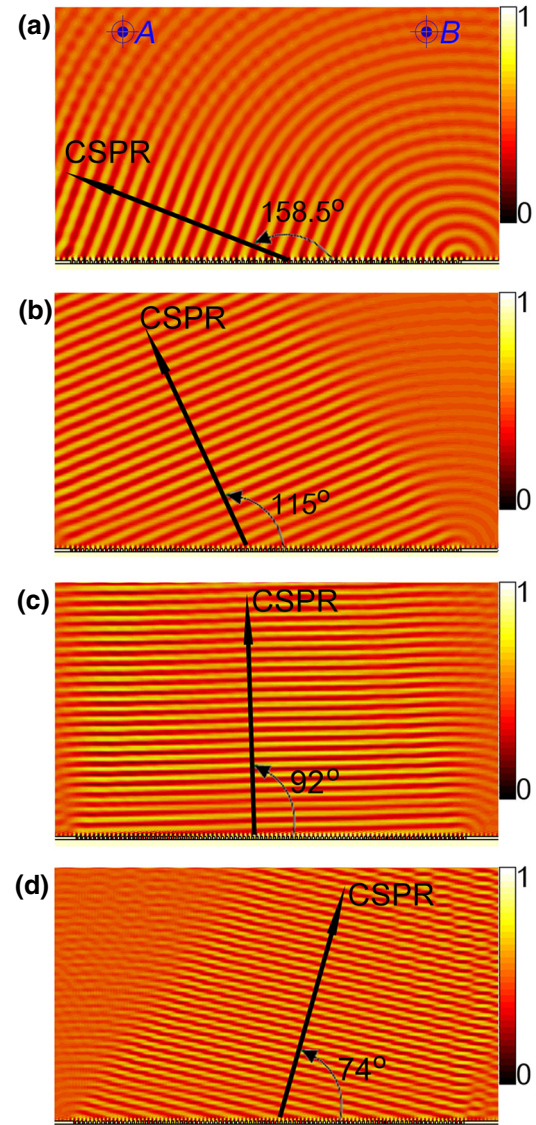


FIG. 5. Field patterns of the E_z component above the second grating for different radiation harmonics. (a)–(d) The sixth, seventh, eighth, and ninth harmonics, respectively. Points A and B in subplot (a) are the positions of the detectors.

most available compact terahertz sources. Here, we only consider properties (frequency and power) of the radiator (source), while the receiving scheme is still important for the radiation actually obtained in practice. Since the radiation direction of SPR changes with the energy of FEB and with frequency, one cannot get all the radiations with different frequencies from the whole grating by using a single detector located far from the grating in experiments. In practice, reflection mirrors need to be used to collect the radiation from the whole grating [31,32]. Also, the radiations with different frequencies at different directions can be received by adjusting the angles of mirrors. To confirm the advantages of the present scheme, we would like

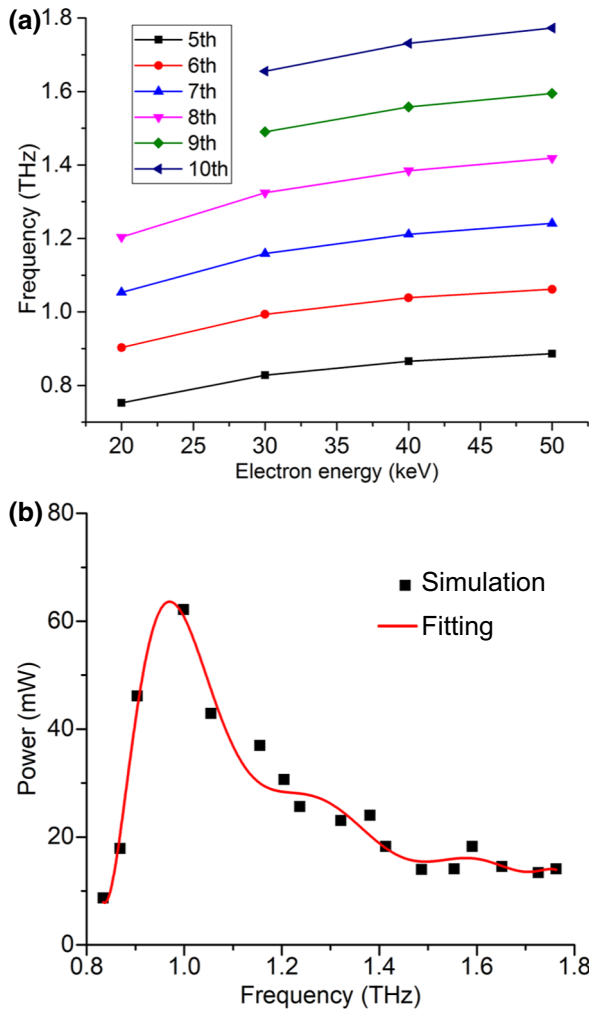


FIG. 6. (a) Dependencies of radiation frequencies on the electron energy of the FEB. (b) Radiation power versus frequency as the beam energy is being tuned.

to compare the simulation results of the present model with those of single-grating models. First, we look at the case that the first grating is absent. Simulations show that, without prebunching, the starting current density should be higher than 200 A/cm^2 on the second grating for the same model. According to previous theories on the SPFEL, the starting current could be reduced by increasing the period number [33,34]. Simulation results indicate that it could be reduced to be less than 150 A/cm^2 when the period number is more than 150, which is still beyond the emission capability of available cathodes. Then, we consider the case that the second grating parameters are replaced by that of the first grating; namely, the second grating is absent. Figure 7(a) presents the spectra of the beam current density of the FEB in the downstream of this model. Compared with the results in Fig. 3(c), the bunching factors of high harmonics are enhanced by interacting with the first grating for a longer distance; yet, they are still much less than that

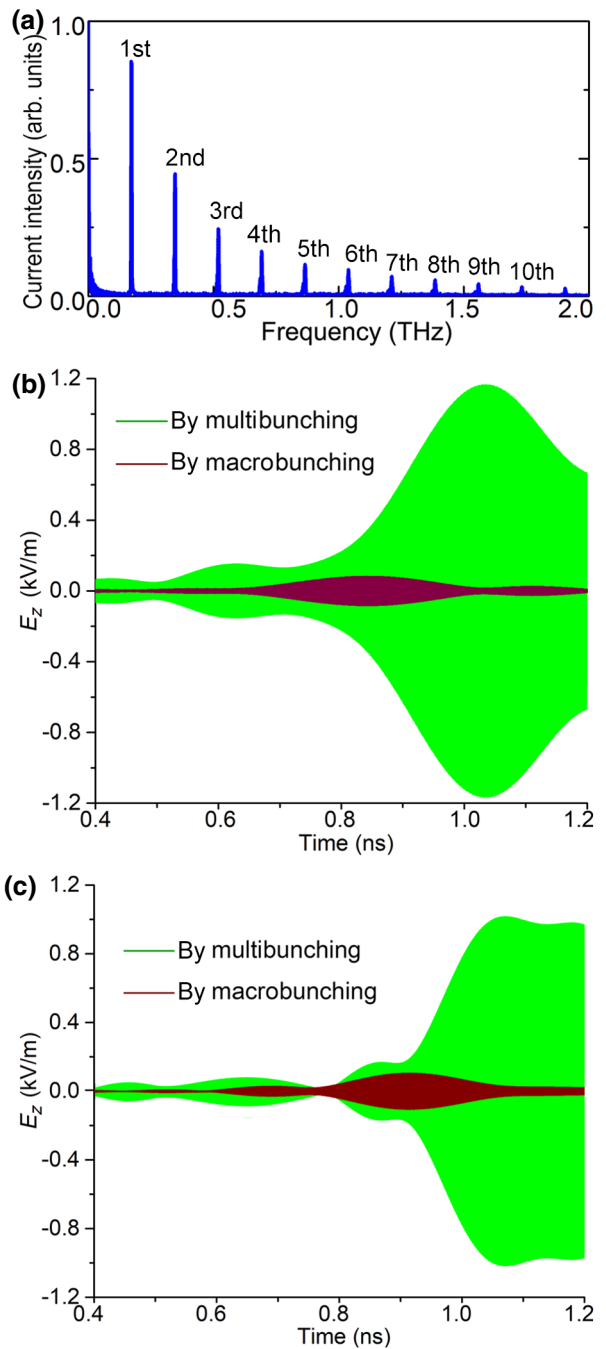


FIG. 7. (a) Frequency spectra of the beam current density of FEB modulated by the first grating. (b),(c) The radiation fields (E_z) of the seventh and eighth harmonics, respectively.

in the multibunching case. Figures 7(b) and 7(c) show the radiation fields (E_z) in the time domain, respectively, from the seventh and eighth harmonics for two models. Here, the fields are filtered to get the objective harmonic component. We note that the radiation field intensity is enhanced by about ten times in the multibunching model, indicating that the radiation power is 2 orders of magnitude increased. Note that the radiation intensity of the SPR is not linearly

proportional to the bunching factor of the FEB. Even the same electron beam generates different radiation intensities, which depend equally on the grating parameters. One of the critical factors is the radiation order (n) given in Eq. (3): the radiation intensity decreases as the radiation order ($|n|$) increases. For the present model, the radiation order of the seventh and eighth harmonics from the second grating is $|n| = 1$, which is the dominant part of the SPR, while those from the first grating are $|n| \geq 3$ and $|n| \geq 4$ [35], respectively.

To verify our main results, we further carried out the three-dimensional (3D) simulations by using the commercial simulation code CST particle studio [36]. Some of the results are shown in Fig. 8, in which the y -directional widths (ignored in the 2D simulations) of grating and of the FEB are both set to be 1.2 mm, without loss of generality, and all other parameters follow that given in Fig. 3.

Figure 8(a) shows the phase-space (energy- z) distribution of the FEB, which is first modulated on the first grating and then further modulated at high harmonics on the second grating, agreeing well with that in Fig. 3(a). The energy and density distributions of particles within the FEB are presented in Fig. 8(b), which shows the bunching processes on both gratings. Figure 8(c) illustrates the field pattern of the E_z component (in the middle x - z cut plane) after the multibunching is achieved. Here, the fields are shown in the time domain ($t = 1.2$ ns), rather than in the frequency domain as given in Fig. 5. We can see that the superradiant SPRs with planar wavefronts are obviously achieved from the second grating. The sixth and seventh harmonics are most remarkable since they are major parts in the radiation. Their radiation directions agree well with that shown in Fig. 5 and theoretical results based on Eq. (3). We also note that the fifth harmonic,

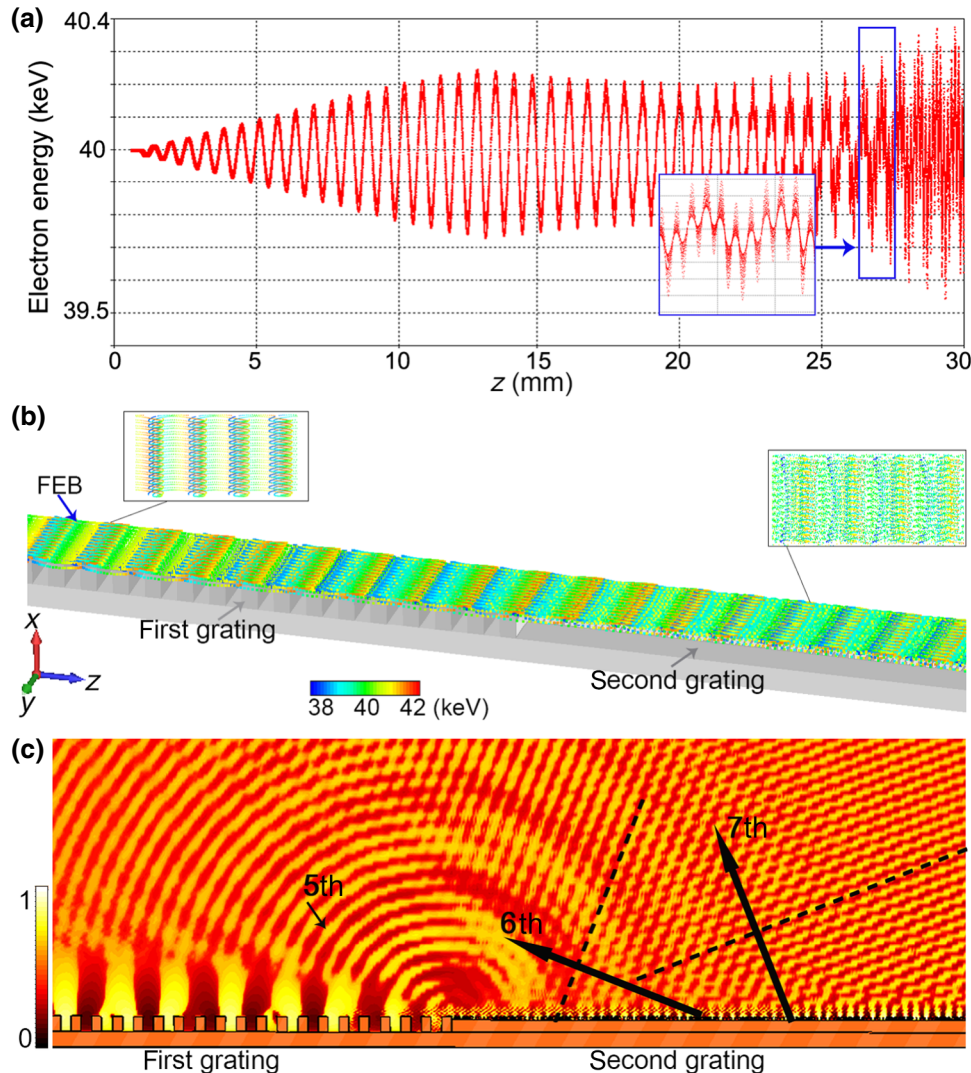


FIG. 8. Simulation results obtained by using CST particle studio. (a) Phase-space distribution of the FEB with modulations. (b) Density and energy distributions of particles within the FEB in the 3D space. (c) Field pattern of the E_z component in x - z cut plane.

which is the surface wave on the second grating, radiates into space through the end of the grating due to the abrupt change of boundary, agreeing with our previous predictions.

V. DISCUSSION AND CONCLUSION

In this section, we discuss several critical factors that affect the operation of the proposed scheme. We first look at the effects of the FEB properties, which are essential for any FEB-driven devices. Figure 9(a) illustrates the dependencies of the simulation-obtained surface-wave intensity (E_z) and of the theoretically calculated growth rate [based on Eq. (19)] on the initial beam-to-grating distance s (here other simulation parameters follow that given in Fig. 3). It shows that the field intensity decreases exponentially as s increases, so it can be understood that the incident fields of the FEB decrease exponentially in the transverse direction of beam velocity [24]. The growth rates on both gratings decrease almost linearly with s , which also indicates that the beam-wave interaction decreases exponentially with s , since the growth rate is in the exponent part of the field expressions. We find that when s is larger than 0.03 mm, the self-bunching cannot be achieved on the second grating. It should be noted that here s denotes the initial beam-to-grating distance. When the beam-wave interaction is started, some electrons transversely deflect due to the self-excited electromagnetic fields and even strike on (scrape) the gratings since the initial beam-to-grating distance (s) is so small. In all our simulations, these effects are considered and the electrons hitting on the gratings are killed. The results show that the scraping of the FEB on gratings does not significantly affect the beam-wave interactions for the considered models. We note that, in some circumstances, the scraping is not necessarily harmful and it may even be helpful for the beam-wave interaction, as illustrated in Refs. [37,38]. Since the beam power (energy and current) considered here is relatively low compared with accelerator-based particles, the scraping does not cause substantial damage to the grating.

Figure 9(b) presents the dependencies of the field intensity (E_z) and of the growth rate on the beam current density. As expected, both of them increase with the beam current density. Also, the growth rates are largely in proportion to the power of 1/3 of the beam current, agreeing with the results given in Ref. [14]. We note that, in order to get the same growth rate on two gratings, the beam current density of the FEB on the second grating should be at least two times larger than that on the first grating. The gain length, which is the reciprocal of the growth rate ($L_g = 1/\tau$), of the first grating is about 1.8 mm (4.5 periods) when the beam current density is 50 A/cm², while that of the second one is about 2.4 mm (30 periods). Namely, to get the same gain, the period number of the second

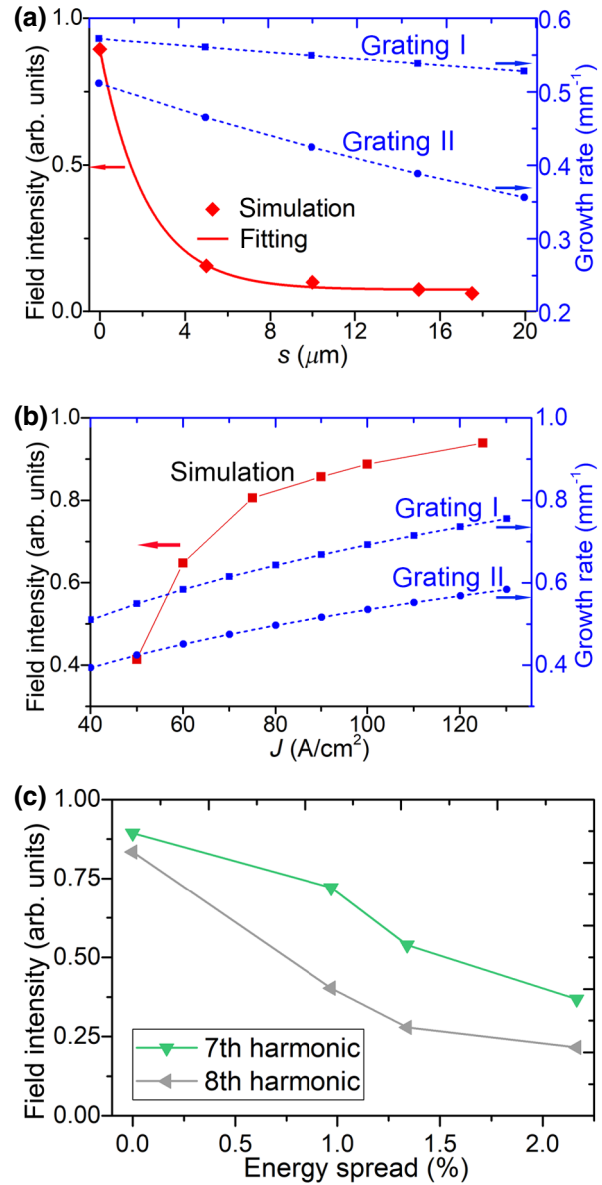


FIG. 9. Dependencies of the simulation-obtained surface-wave intensity (E_z) and of the theoretically calculated growth rate on the beam-to-grating distance s (a) and the beam current density (b). In subplot (a), the exponential fitting is used for the simulation results. (c) Dependencies of the simulation-obtained radiation-field intensities on the initial energy spread of the FEB.

grating should be six times more than that of the first grating.

Another important factor is the initial energy spread (IES) of the FEB. In simulations, we preset the initial particle velocities of the FEB to follow the Maxwellian distribution, which is according to actual properties of the FEB from electron guns with thermionic cathodes [39,40]. Simulation-obtained radiation intensity versus IES is presented in Fig. 9(c), which shows that the field intensity decreases steadily as the IES increases. Further simulations

show that the self-bunching cannot be started as the IES reaches 2%.

Additionally, in order to get a well-prebunched FEB, which is of significance for the operation of the proposed scheme, the FEB and the first grating should match well. The first grating should not be too short; otherwise, the prebunching cannot be achieved. It should not be too long either; otherwise, the FEB is overbunched, which degrades the performance. Besides overbunching, the increase of beam energy spread after the saturation of the beam-wave interaction on the first grating also greatly affects the operation of the second grating. For the present model with a beam current density of 50 A/cm^2 and beam-to-grating distance of 0.01 mm, we find that the optimum length of the first grating is about 45 periods ($10L_g$).

It is worth noting that the proposed scheme can also be applied to cylindrical gratings with hollow electron beams, similarly to the previous cylindrical SPFELs presented in Refs. [21] and [23]. Compared with the sheet electron beam used in the planar model, the cylindrical hollow electron beams are easier to control, since they are axial symmetric. Yet, the cylindrical gratings are more difficult to manufacture in the terahertz region and the power is relatively low. On the contrary, planar gratings are easier to manufacture and their power capacity can be improved by increasing the transverse (y -directional) widths of the grating and of the electron beam. Yet, the sheet electron beam is more difficult to form and sustain since the electrons at fringes (lateral sides) of the beam encounter a more significant space-charge effect and deflect more seriously, resulting in the deformation of the beam. To avoid this situation, a stronger guiding magnetic field has to be used to confine the sheet beams in practice.

Lastly, we would like to discuss the prebunching method of the proposed scheme. As is known, many other techniques could be used for prebunching the FEB, such as using kickers and rf resonators. Yet, in the present model, the prebunching frequency is as high as 0.17 THz, which exerts a great challenge on the kickers, whose operating frequency is usually less than several GHz. It is not easy for the rf resonators to reach such a high frequency either because of the manufacture difficulties of very small cavities. Comparatively, the planar grating used in the present scheme is not difficult for fabrication. Another method of generating a prebunched beam is using a train of laser pulses to drive a photocathode, which could generate a train of electron bunches with bunching frequency reaching 1 THz [41]. Yet, this method can only generate tens of bunches within a train, which is much less than the number of bunches in the present method. Also, the present one is much more compact and easier to realize than this mentioned method.

In conclusion, we propose and investigate a terahertz frequency mixer by multibunching a free-electron beam on two cascade gratings. The free-electron beam is first

macrobunched at a low frequency on the first grating and then microbunched at a high frequency on the second grating, producing a series of frequency-mixed bunches within the beam. The multibunched beam can generate multicolor coherent terahertz radiation via the superradiant Smith-Purcell effect. Also, the radiation frequency can be tuned from 0.8 to 1.8 THz by changing the beam energy from 20 to 50 keV. It is an efficient way of generating multicolor and broad-tunable terahertz radiation in practice.

ACKNOWLEDGMENTS

This work is supported by Natural Science Foundation of China (Grants No. 61471332, No. 51627901, and No. U1632150) and Chinese Universities Scientific Fund (Grant No. WK2310000059).

- [1] M. Tonouchi, Cutting-edge terahertz technology, *Nat. Photonics* **1**, 97 (2007).
- [2] Q. Y. Wu, H. Tanoto, L. Ding, C. C. Chum, B. Wang, A. B. Chew, A. Banas, K. Banas, S. J. Chua, and J. Teng, Branch-like nano-electrodes for enhanced terahertz emission in photomixers, *Nanotechnology* **26**, 255201 (2015).
- [3] R. Kowerdziej, M. Oliferczuk, J. Parka, and J. Wróbel, Terahertz characterization of tunable metamaterial based on electrically controlled nematic liquid crystal, *Appl. Phys. Lett.* **105**, 022908 (2014).
- [4] N. Laman, M. Bieler, and H. M. van Driel, Ultrafast shift and injection currents observed in wurtzite semiconductors via emitted terahertz radiation, *J. Appl. Phys.* **98**, 103507 (2005).
- [5] A. Maestrini, I. Mehdi, J. V. Siles, J. S. Ward, R. Lin, B. Thomas, C. Lee, J. Gill, G. Chattopadhyay, E. Schlecht, J. Pearson, and Peter Siegel, Design and characterization of a room temperature all-solid-state electronic source tunable from 2.48 to 2.75 THz, *IEEE Trans. Terahertz Sci. Technol.* **2**, 177 (2012).
- [6] M. Philipp, U. U. Graf, A. Wagner-Gentner, D. Rabanus, and F. Lewen, Compact 1.9 THz BWO local-oscillator for the GREAT heterodyne receiver, *Infr. Phys. Technol.* **51**, 54 (2007).
- [7] M. Mineo and C. Paoloni, Corrugated rectangular waveguide tunable backward wave oscillator for terahertz applications, *IEEE Trans. Electron Devices* **57**, 1481 (2010).
- [8] J. H. Booske, R. J. Dobbs, C. D. Joye, C. L. Kory, G. R. Neil, G.-S. Park, J. Park, and R. J. Temkin, Vacuum electronic high power terahertz sources, *IEEE Trans. Terahertz Sci. Technol.* **1**, 54 (2011).
- [9] W. He, L. Zhang, D. Bowes, H. Yin, K. Ronald, A. D. R. Phelps, and A. W. Cross, Generation of broadband terahertz radiation using a backward wave oscillator and pseudospark-sourced electron beam, *Appl. Phys. Lett.* **107**, 133501 (2015).
- [10] W. Liu and Z. Xu, Simulations of table-top watt-class 1-THz radiation sources with two-section periodic structure, *J. Appl. Phys.* **115**, 014503 (2014).

- [11] P. Makhalov and A. Fedotov, Design and modeling of a slow-wave 260 GHz tripler, *IEEE Trans. THz Sci. Technol.* **5**, 1048 (2015).
- [12] S. J. Smith and E. M. Purcell, Visible light from localized surface charges moving across a grating, *Phys. Rev.* **92**, 1069 (1953).
- [13] J. Urata, M. Goldstein, M. F. Kimmitt, A. Naumov, C. Platt, and J. E. Walsh, Superradiant Smith-Purcell Emission, *Phys. Rev. Lett.* **80**, 516 (1998).
- [14] H. L. Andrews and C. A. Brau, Gain of a Smith-Purcell free-electron laser, *Phys. Rev. ST Accel. Beams* **7**, 070701 (2004).
- [15] A. Tavousi, A. Rostami, G. Rostami, and M. Dolatyari, Smith-Purcell based terahertz frequency multiplier: Three dimensional analysis, *Photoptics* **2015**, 145 (2016).
- [16] Yu. A. Grishin, M. R. Fuchs, A. Schnegg, A. A. Dubinskii, B. S. Dumesh, F. S. Rusin, V. L. Bratman, and K. Mobius, Pulsed OrotronA new microwave source for submillimeter pulse high-field electron paramagnetic resonance spectroscopy, *Rev. Sci. Instrum.* **75**, 2926 (2004).
- [17] G. S. Nusinovich, Analytical nonlinear theory of the orotron, *Phys. Plasmas* **13**, 053107 (2006).
- [18] M. Cao, W. Liu, Y. Wang, and K. Li, Three-dimensional theory of Smith-Purcell free-electron laser with dielectric loaded grating, *J. Appl. Phys.* **116**, 103104 (2014).
- [19] J. Gardelle, P. Modin, and J. T. Donohue, Start Current and Gain Measurements for a Smith-Purcell Free-Electron Laser, *Phys. Rev. Lett.* **105**, 224801 (2010).
- [20] K. B. Oganesyan, Smith-Purcell radiation amplifier, *Laser Phys. Lett.* **12**, 116002 (2015).
- [21] J. Gardelle, P. Modin, H. P. Bluem, R. H. Jackson, J. D. Jarvis, A. M. M. Todd, and J. T. Donohue, A compact THz source: 100/200 GHz operation of a cylindrical Smith-Purcell free-electron laser, *IEEE Trans. THz Sci. Technol.* **6**, 497 (2016).
- [22] C. Prokop, P. Piot, M. C. Lin, and P. Stoltz, Numerical modeling of a table-top tunable SmithCPurcell terahertz free-electron laser operating in the super-radiant regime, *Appl. Phys. Lett.* **96**, 151502 (2010).
- [23] L. Liang, W. Liu, Q. Jia, L. Wang, and Y. Lu, High-harmonic terahertz Smith-Purcell free-electron-laser with two tandem cylindrical-gratings, *Opt. Express* **25**, 2960 (2017).
- [24] H. L. Andrews, C. H. Boulware, C. A. Brau, and J. D. Jarvis, Superradiant emission of Smith-Purcell radiation, *Phys. Rev. ST Accel. Beams* **8**, 110702 (2005).
- [25] D. Y. Sergeeva, A. P. Potylitsyn, A. A. Tishchenko, and M. N. Strikhanov, Smith-Purcell radiation from periodic beams, *Opt. Express* **25**, 26310 (2017).
- [26] K. Zhang and D. Li, *Electromagnetic Theory in Microwave and Optoelectronics* (Springer-Velag, Berlin/Heidelberg, 2008).
- [27] J. Zhou, D. Liu, C. Liao, and Z. Li, CHIPIC: An efficient code for electromagnetic PIC modeling and simulation, *IEEE Trans. Plasma Sci.* **37**, 2002 (2009).
- [28] A. Srivastava, J.-K. So, Y. Wang, J. Wang, R. S. Raju, S.-T. Han, G.-S. Park, Design of sheet-beam electron gun with planar cathode for terahertz devices, *J Infrared Milli Terahz Waves* **30**, 670 (2009).
- [29] D. H. Shin, K. N. Yun, J. S. Han, C. J. Lee, S.-G. Jeon, and D. Shin, in *Proceedings of the 28th International Vacuum Nanoelectronics Conference (IVNC), Guangzhou, 2015*, edited by S. Deng, J. She, J. Chen, Q. Zou and P. Ye (Sun Yat-Sen University, Guangzhou, 2015), p. 216.
- [30] L. Li, J. Wang, and Y. Wang, Generation of high-current-density sheet electron beams, *IEEE Electron Device Lett.* **30**, 228 (2009).
- [31] S. E. Korbyl, A. S. Kesar, J. R. Sirigiri, and R. J. Temkin, Observation of Frequency-Locked Coherent Terahertz Smith-Purcell Radiation, *Phys. Rev. Lett.* **94**, 054803 (2005).
- [32] Y. Shibata, S. Hasebe, K. Ishi, S. Ono, M. Ikezawa, T. Nakazato, M. Oyamada, S. Urasawa, T. Takahashi, T. Matsuyama, K. Kobayashi, and Y. Fujita, Coherent Smith-Purcell radiation in the millimeter-wave region from a short-bunch beam of relativistic electrons, *Phys. Rev. E* **57**, 1061 (1998).
- [33] V. Kumar and K. J. Kim, Analysis of Smith-Purcell free-electron lasers, *Phys. Rev. E* **73**, 026501 (2006).
- [34] W. Liu, M. Cao, Y. Wang, and K. Li, Start current of dielectric-loaded grating in Smith-Purcell radiation, *Phys. Plasmas* **23**, 033104 (2016).
- [35] According to Eq. (3), $|n| \geq 3$ has to be satisfied for the 7th harmonic to generate Smith-Purcell relation from the first grating, and for the same reason, $|n| \geq 4$ has to be satisfied for the 8th harmonic.
- [36] CST Corp., CST PS Tutorials, <http://www.cst-china.cn/>.
- [37] K. Schunemann and D. M. Vavrik, Theory of the clinotron: A grating backward-wave oscillator with inclined electron beam, *IEEE Trans. Electron Devices* **46**, 2245 (1999).
- [38] M. Sattorov, E. Khutoryan, K. Lukin, O. Kwon, and G. S. Park, Improved efficiency of backward-wave oscillator with an inclined electron beam, *IEEE Trans. Electron Devices* **60**, 458 (2013).
- [39] L. H. Germer, The distribution of initial velocities among thermionic electrons, *Phys. Rev.* **25**, 795 (1925).
- [40] B. Goplen, L. Ludeking, D. Smith, and G. Warren, User-configurable MAGIC for electromagnetic PIC calculations, *Comput. Phys. Commun.* **87**, 54 (1995).
- [41] Y.-C. Huang, Desktop megawatt superradiant free-electron laser at terahertz frequencies, *Appl. Phys. Lett.* **96**, 231503 (2010).